九州工業大学学術機関リポジトリ

## Kyutacar

Kyushu Institute of Technology Academic Repository

# Strong suppression of Curie temperature of spin-polarized ferromagnet La1-xSrxMnO3 by application of dynamic strain

# Strong suppression of Curie temperature of spin-polarized ferromagnet La$_{1-x}$Sr$_x$MnO$_3$ by application of dynamic strain

M. Mito (iD), K. Tsuruta (iD), T. Tajiri (iD), N. Ikeda, M. Ohkuma, A. Kohno, K. Konishi (iD), and H. Deguchi

# Strong suppression of Curie temperature of spin-polarized ferromagnet La$_{1-x}$Sr$_x$MnO$_3$ by application of dynamic strain

View Online          Export Citation          CrossMark

M. Mito,[1,a] K. Tsuruta,[2] T. Tajiri,[3,b] N. Ikeda,[1] M. Ohkuma,[1] A. Kohno,[3] K. Konishi,[4] and H. Deguchi[1]

AFFILIATIONS

[1] Faculty of Engineering, Kyushu Institute of Technology, Kitakyushu 804-8550, Japan
[2] Japan Synchrotron Radiation Research Institute (JASRI), Hyogo 679-5198, Japan
[3] Faculty of Science, Fukuoka University, Fukuoka 814-0180, Japan
[4] Graduate School of Science and Engineering, Ehime University, Matsuyama 790-8577, Japan

[a] Author to whom correspondence should be addressed: mitoh@mns.kyutech.ac.jp
[b] Electronic mail: tajiri@fukuoka-u.ac.jp

ABSTRACT

The ferromagnetic state of the spin-polarized ferromagnet La$_{1-x}$Sr$_x$MnO$_3$ is stabilized in the metallic region by strong coupling between localized spins in the $t_{2g}$ orbital and conduction electrons in the $e_g$ orbital. We prepared polycrystalline La$_{1-x}$Sr$_x$MnO$_3$ films ($x = 0.15, 0.25,$ or 0.30) by deposition on an oxidized Si substrate. The three types of La$_{1-x}$Sr$_x$MnO$_3$ films were in the ferromagnetic rhombohedral phase, and their Curie temperatures, $T_C$, evaluated from the midpoint of ac magnetization, were 305 K, 335 K, and 338 K, respectively. By applying expansion-mode acoustic vibration to the crystal structure of La$_{1-x}$Sr$_x$MnO$_3$, we observed a remarkable decrease (as large as 70 K) in $T_C$. The applied structural perturbation causes a decrease in the possibility of conduction electron hopping and an increase in the Jahn–Teller distortion. The former is more effective for decreasing $T_C$ than the latter.

## I. INTRODUCTION

External fields such as a magnetic field $H$, an electric field $E$, and a force tensor $\sigma$ are associated with physical quantities such as magnetization $M$, electric polarization (electrical conductivity) $P$, and a strain tensor $\epsilon$, respectively. Between the external field and the corresponding quantity, there are defined susceptibilities that exhibit linearity, that is, $M/H$, $P/E$, and $\epsilon/\sigma$. Multiferroic materials can be controlled in two ways, by changing $P$ via $H$ and changing $M$ via $E$ in addition to directly changing $M$ via $H$ and changing $P$ via $E$. These cross-relationships expand the functionality of electronic materials and spintronic materials. Measurements of $M$ and/or $P$ as a function of $\sigma$, in so-called high-pressure (HP) experiments, may be considered a static type of cross-relationship because the electronic functionality originates from a crystal structure with translation symmetry.

The spin-polarized ferromagnet La$_{1-x}$Sr$_x$MnO$_3$ is a type of perovskite Mn oxide. In the perovskite structure, La and Sr atoms are located at the A site, whereas Mn is located at the B site.[1] In 1950, Jonker and Santen found that the ferromagnetic (FM) phase of La$_{1-x}$Sr$_x$MnO$_3$ appeared in a metallic phase stabilized by doping holes.[2] Motivated by the above study, researchers have investigated the phase diagram as a function of the hole concentration.[3,4] In 2002, Hemberger et al. conducted detailed investigations of the structural and magnetic phase diagram of the crystalline material as a function of the hole concentration.[5] La$_{1-x}$Sr$_x$MnO$_3$ exhibits various crystal structures, including orthorhombic, rhombohedral, tetragonal, monoclinic, and hexagonal structures, depending on the temperature and Sr concentration. The FM state is stabilized via the structural transformation from orthorhombic to rhombohedral structure, where the insulating state changes to a metallic one. At zero temperature, the orthorhombic insulating FM phase appears
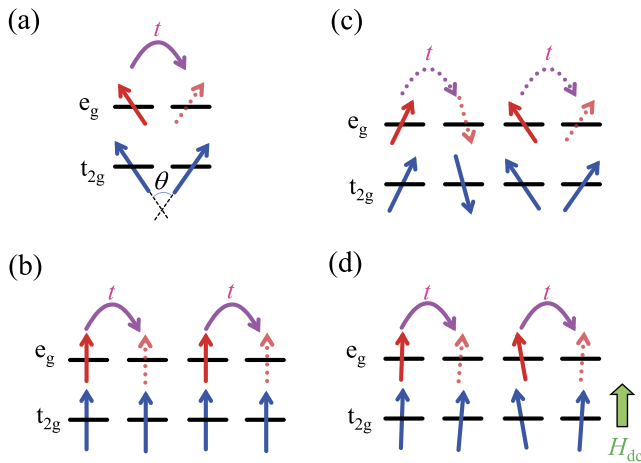
**FIG. 1**. Overview of the mechanism of double exchange interaction in $La_{1-x}Sr_xMnO_3$ with the electron configuration of $t_{2g}^3 e_g^1$, drawn referring to the content of Ref. [9]. Here, $e_g$ and $t_{2g}$ are singlet and triplet states, respectively. (a) Schematic of the double exchange interaction for two $Mn^{3+}$ sites. The magnitude of the charge transfer integral $t$ is proportional to $\cos(\theta/2)$, where $\theta$ is the angle between the spins on $t_{2g}$.[6] [(b)–(d)] Schematics of the many-body system of $Mn^{3+}$ ions for (b) $T < T_C$ and (c) $T > T_C$ and a dc magnetic field $H_{dc} = 0$, and (d) $T > T_C$ and $H_{dc} > 0$.

for $x = 0.10$–$0.17$, and it changes to the rhombohedral metallic FM phase for $x = 0.21$–$0.49$ through the orthorhombic metallic FM phase for $x = 0.17$–$0.21$. The crystal field splits the energy levels of $Mn^{3+}$ into two levels, such as the singlet $e_g$ and triplet $t_{2g}$, as shown in Fig. 1. One-half the spin of a conduction electron on $e_g$ is ferromagnetically coupled by Hund coupling with the spin of three halves on $t_{2g}$, resulting in a spin of four halves at the same site. Sr is substituted at the La site, so holes are doped into $e_g$ [Fig. 1(a)]. The holes can hop into neighboring $e_g$ levels. The magnitude of the charge transfer integral $t$ is proportional to $\cos(\theta/2)$, where $\theta$ is the angle between spins on $t_{2g}$, as shown in Fig. 1(a).[6] This conduction electron is strongly coupled with the localized spins of $Mn^{3+}$,[7] so the electrical conductivity over $Mn^{3+}$ ions influences the magnetic order, as illustrated in Figs. 1(b) (FM for large $t$) and 1(c) (non-FM for small $t$). Thus, the magnetic correlation between $Mn^{3+}$ ions has been understood within the framework of a double exchange

interaction.[8,9] As a result, when an external dc magnetic field $H_{dc}$ stabilizes the FM alignment, even above the magnetic ordering temperature ($T_C$), the electron–spin coupling enhances the mobility of the conduction electron, as illustrated in Fig. 1(d). Consequently, this strong correlation also causes the giant magnetoresistance effect in the insulating region ($x < 0.15$) under $H_{dc}$.[10,11]

This magneto-structural correlation has been studied using the lattice mismatch between epitaxial films and the substrate,[12–16] chemical pressure,[17–20] and HP compression of bulk samples[21–23] (see Table I). The chemical pressure obtained by substituting rare-earth cations with different radii causes an increase in $T_C$.[17–20] In 1995, Moritomo *et al.* reported that the temperature dependence of electrical resistance and magnetization for $x = 0.15$–$0.40$ under hydrostatic pressure.[21] For instance, increases in the FM transition Curie temperature $T_C$ are observed as follows: $\Delta T_C = 14.2$ K at 0.90 GPa for $x = 0.15$ ($dT_C/dP = 15.8$ K/GPa), $\Delta T_C = 7.5$ K at 0.80 GPa for $x = 0.20$ ($dT_C/dP = 9.4$ K/GPa), and $\Delta T_C = 2.6$ K at 0.52 GPa for $x = 0.30$ ($dT_C/dP = 5.3$ K/GPa). For lower initial $T_C$ values, $dT_C/dP$ is larger. The insulating FM phase at $x = 0.15$ exhibits a larger increase in $T_C$ under pressure than the metallic FM phase at $x = 0.30$. In 1998, Millis *et al.* explained that hydrostatic compression (expansion) will increase (decrease) the electron hopping amplitude and thereby reduce (increase) the electron lattice coupling, resulting in higher (lower) $T_C$ values.[24] By contrast, biaxial or shear strain increases the energy difference between the $e_g$ levels imposed by Jahn–Teller distortion, reinforcing the tendency of electrons to be localized, and thus reducing $T_C$.[24]

Furthermore, the response to anisotropic structural modification accompanied by tensile and compressive strains is opposite to that under hydrostatic pressure.[25] In an FM metal for $x = 0.30$, piezo-elastic strain (PES) of $+0.90\%$ along [100], $-0.23\%$ along [01$\bar{1}$], and $-0.70\%$ along [011] causes $T_C$ to decrease by as much as $\Delta T_C = -10$ K,[25] the magnitude of which is larger than that under HP compression for $x = 0.30$ (see Table I). This observation suggests that the change in $T_C$ depends on the type of structural change, i.e., hydrostatic compression or anisotropic compression accompanied by tensile and compressive strains. In particular, for thin films, the structural modification can enhance the controllability of the magnetic properties, in particular, that of epitaxial heterostructures, when an electric field is applied.[26,27] There is surely a lattice parameter mismatch between $La_{1-x}Sr_xMnO_3$ and the substrate, which appears as a static strain, and the additional static stress further enhances the controllability owing to a remarkable change in $T_C$.

**TABLE I**. Previous studies of strain response on $La_{1-x}Sr_xMnO_3$. HP and PES stand for high-pressure compression and piezo-elastic strain, respectively. $T_C$ is evaluated from the offset temperature of the magnetic signal. *1 expresses the state with $+0.90\%$ along [100], $-0.23\%$ along [00$\bar{1}$], and $-0.70\%$ along [011].

| $x$ | Type of experiment | Initial $T_C$ (K) | $\Delta T_C$ | $dT_C/dP$ (K/GPa) | Reference |
|---|---|---|---|---|---|
| $x = 0.15$ | HP | 244 | 14.2 K at 0.90 GPa | 15.8 | 21 |
| $x = 0.20$ | HP | 314 | 7.5 K at 0.80 GPa | 9.4 | 21 |
| $x = 0.25$ | HP | 342 | 4.7 K at 0.64 GPa | 7.3 | 21 |
| $x = 0.30$ | HP | 359 | 2.6 K at 0.52 GPa | 5.3 | 21 |
| $x = 0.30$ | HP | 370 | 25 K at 5.8 GPa | 4.3 | 22 |
| $x = 0.30$ | PES | . . . | ca. $-10$ K (*1) | . . . | 25 |

To obtain useful devices in the future, as an additional structural modulation, not static but dynamic is favorable. A possible perturbation method is the use of ultrasonic waves along with shock waves. In this case, stress should be applied as a function of time. Furthermore, dynamic stress results in diffusive acoustic strain. In this study on $La_{1-x}Sr_xMnO_3$ films, we expect a very large switching response, as shown in Figs. 1(b) and 1(c), owing to enhanced electron scattering.

## II. EXPERIMENTAL METHODS

Polycrystalline $La_{1-x}Sr_xMnO_3$ films ($x$ = 0.15, 0.25, and 0.30) were deposited on oxidized Si as follows: The Si substrate was oxidized to insulate the $La_{1-x}Sr_xMnO_3$ film from the Si substrate. The value of $x$ in $La_{1-x}Sr_xMnO_3$ is the charge value of Sr in the preparation stage. The synthesized precursor solutions, which were stoichiometric ethanol solutions of $LaCl_3 \cdot 7H_2O$, $SrCl_2 \cdot 6H_2O$, and $MnCl_2 \cdot 4H_2O$, were coated on the thermally oxidized p-type Si (100) $[SiO_2/p-Si(100)]$ substrate by dip coating. The solution-coated substrates were dried and calcined. Cross-sectional observations by scanning electron microscopy (SEM) indicated that the polycrystalline $La_{1-x}Sr_xMnO_3$ films were approximately 7 $\mu$m thick. The electrical resistance $R$ at room temperature was obtained from the $I–V$ behavior in the region up to $I$ = 1 mA observed by a wafer prober. The distance between electrodes was ~3.3 mm. The $R$ value at room temperature, estimated in the state of ohmic contact, is 48.0 kΩ for $x$ = 0.15 kΩ, 21.0 kΩ for $x$ = 0.25 kΩ, and 15.1 kΩ for $x$ = 0.30. Thus, $R$ decreased with increasing $x$. All three polycrystalline films exhibit the ferromagnetic behavior above room temperature, suggesting the existence of the metallic phase. However, their resistivity is in the order of 0.1 Ωm. The SEM picture reveals that inhomogeneity existed at the grain level and the metallic phase would be mixed in a magnetically disordered insulating matrix. In particular, the characteristic ac magnetization at $x$ = 0.15 is observed over a wide temperature range owing to non-negligible inhomogeneity, as seen in $LaSr_{0.3}MnO_3$ films deposited on Si by pulsed laser deposition.[28] Thus, the effective hole concentration for the $x$ = 0.15

film is assumed to correspond to that for $x \sim 0.18$ according to the temperature dependence of the ac magnetization.[21]

Figure 2 shows the experimental setup for applying dynamic strain,[29,30] which can be inserted into low-temperature equipment such as a commercial superconducting quantum interference device (SQUID) magnetometer. The actuator (Murata Manufacturing, CSBLA1M00J58-B0) is packaged with the insulating body, as shown in Figs. 2(a) and 2(b), which is convenient for insulating the actuator from the film. The packaged actuator is $6 \times 5 \times 2$ mm$^3$ in size. The mechanical vibration of the piezoelectric transducer (PZT) is transmitted to the actuator package, as shown in Fig. 2(b), resulting in expansion-mode vibration in which out-of-plane compression and out-of-plane tension are repeated at an interval corresponding to the actuation frequency [Fig. 2(c)]. The resonant frequency of the actuator was approximately 1 MHz, and it was finely adjusted at each measurement temperature by seeking the minimum impedance of the actuator using an oscilloscope connected in parallel with the actuator, as shown in Fig. 2(a).[29] The magnitude of the vibration depends on the voltage $V$ applied to both electrodes of the actuator. We cannot entirely ignore the heating effects. According to a test using an infrared thermometer, the heating effect is as high as 20 K at the maximum $V$ (=20 $V_{PP}$), even with no thermal contact with a liquid thermal bath at $^4$He temperature. When there is thermal contact between the actuator and a Cu block, the increase in temperature at approximately room temperature is at most 4 K.[29] Both the X-ray diffraction (XRD) and ac magnetization measurements described below were conducted after reaching a thermal equilibrium state at a certain $V$. XRD experiments detect the static structural information for spatially deformed and time-averaged states, and ac magnetic measurements detect magnetic response against the ac field with 10 Hz for spatially deformed states.

The XRD experiment was conducted using SmartLab (Rigaku) parallel optics with Cu ($K\alpha1$, $K\alpha2$) x-ray radiation at room temperature. The setup shown in Fig. 2 was installed in the diffractometer. The orientation of the crystallites in the films was not isotropic, so the diffraction peaks could not all be observed at the same time.
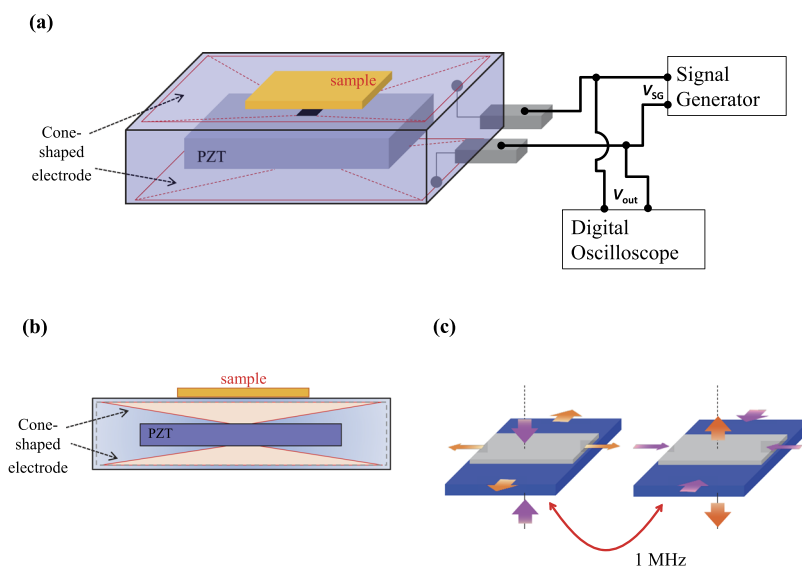


(a)

(b)

(c)

FIG. 2. (a) Overview of the actuating system. (b) Actuator in expanding oscillation mode, with a resonating frequency of 1 MHz (Murata Manufacturing, CSBLA1M00J58-B0) and a surface area of $6 \times 5$ mm$^2$, is packaged with the insulating body. (c) Characteristic actuating modes appearing in expansion-mode vibration.

Thus, for $x = 0.15$, the diffraction peaks of each plane index (104) and (012) were observed. For $x = 0.30$, the diffraction peak of the plane index (300), in addition to that of the (104) plane, was observed. For comparison with previous studies,[22] structural changes at the unit-cell level were obtained via the structural parameters of the hexagonal unit cell estimated assuming a rhombohedral system. The experimental results of XRD analysis and ac magnetization under acoustic strain are presented below.

The ac magnetization was measured using a SQUID magnetometer with an ac option. An ac field with a frequency of 10 Hz and an amplitude of 3.9 Oe was applied. The change in the Curie temperature $T_C$ was evaluated using two characteristic temperatures, that is, the offset and midpoint of the temperature dependence of the ac magnetization. The change in ac magnetization of the actuating unit as a function of temperature is negligible compared to that of the $La_{1-x}Sr_xMnO_3$ films.

## III. EXPERIMENTAL RESULTS

### A. XRD

Figures 3(a) and 3(b) show the changes in the XRD profiles of the (104) plane for $x = 0.15$ and 0.30, respectively, during the
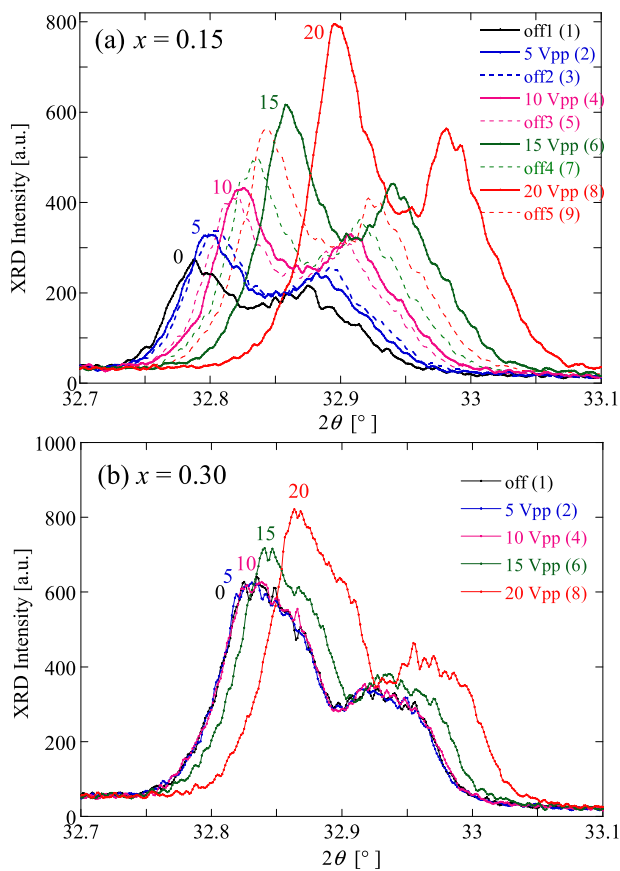
sequence $V = 0$ (1) → 5 (2) → 0 (3) → 10 (4) → 0 (5) → 15 (6) → 0 (7) → 20 (8) → 0 $V_{pp}$ (9). In Fig. 3(b), the shift in the XRD profile is small, and only the data for the initial $V$ value of 0 are presented. Figures 4 and 5 show the $V$ dependence of the lattice constants $a$ and $c$ [Figs. 4(a) and 5(a)] and the Mn–O–Mn bonding angle (∠Mn–O–Mn) and Mn–O bond length [Figs. 4(b) and 5(b)] for $x = 0.15$ and 0.30, respectively. In $R\bar{3}c$, the Mn and O sites are represented as (0, 0, 0) and ($x'$, 0, 1/4), respectively.[31] Both ∠Mn–O–Mn and Mn–O bond lengths are determined uniquely. We determined 0.4489 as the value of $x'$, which is quite similar to that in Ref. 31. Here, the Mn–O bond length and ∠Mn–O–Mn were calculated assuming that the atomic coordination of oxygen does not depend on the voltage applied to the actuator.

For $x = 0.15$, which should be the insulating phase in the well-known phase diagram,[5] $a$ increases and $c$ decreases with increasing $V$. The unit-cell volume increases with increasing $V$, and the increase is as large as 0.06% at $V = 20$ $V_{pp}$. This unit-cell level of structural change is different from that occurring under hydrostatic HP compression accompanied by reduction in both $a$ and $c$. The Mn–O–Mn angle decreases with increasing $V$, whereas the Mn–O bond length changes little. This change in the Mn–O–Mn angle is opposite to the increase toward 180°, favorable to the increase in $T_C$ that occurs under hydrostatic HP compression.[22]

For $x = 0.30$, which is certainly in the metallic FM phase, both $a$ and $c$ decrease with increasing $V$, which is similar to the



**FIG. 3**. XRD profiles of the (104) plane for the $La_{1-x}Sr_xMnO_3$ films with $x = 0.15$ (a) and 0.30 (b). The low-angle and high-angle Bragg peaks are due to Cu K$\alpha$1 and Cu K$\alpha$2 radiation, respectively.



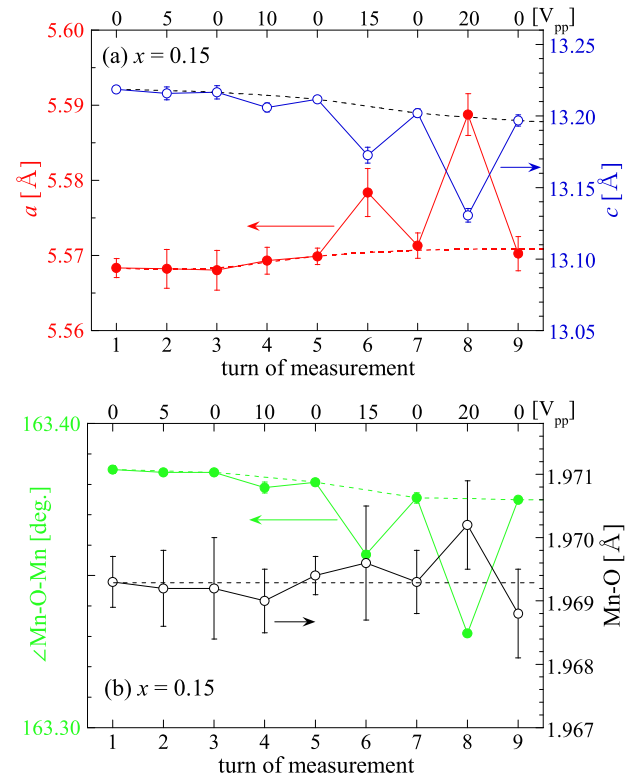**FIG. 4**. Structural parameters of the $La_{1-x}Sr_xMnO_3$ film with $x = 0.15$ determined from the XRD profiles of the (104) and (012) planes. (a) Lattice parameters $a$ and $c$, and (b) ∠Mn–O–Mn and Mn–O bond length.

FIG. 5. Structural parameters of the $La_{1-x}Sr_xMnO_3$ film with $x = 0.30$ determined from the XRD profiles of the (104) and (300) planes. (a) Lattice parameters $a$ and $c$, and (b) ∠Mn–O–Mn and Mn–O bond length.
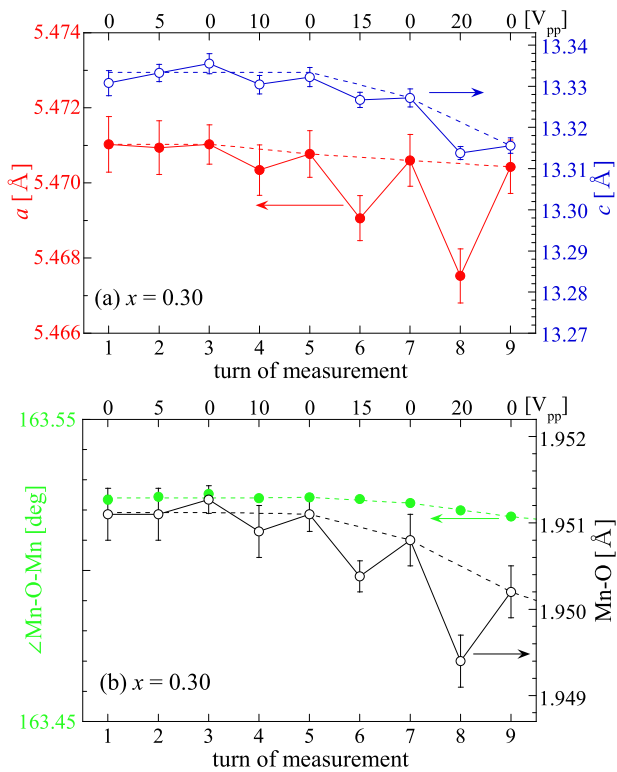
behavior under hydrostatic HP compression.[22] The Mn–O–Mn angle changes little under acoustic strain, whereas the Mn–O bond length decreases with increasing $V$. The unit-cell volume decreases with increasing $V$, and the decrease is as large as 0.26% at $V = 20$ $V_{pp}$, the magnitude of which is more than four times that at $x = 0.15$. At $V = 20$ $V_{pp}$, the ratios of the changes in $a$ and $c$ are −0.06% and −0.13%, respectively, suggesting a quasi-isotropic shrinkage of approximately −0.1%. This behavior is consistent with the observation that ∠Mn–O–Mn changes little under acoustic strain. Thus, if we explain the change in $T_C$ according to the change in the Mn–O–Mn angle in the framework of the double exchange interaction model, the decrease in $T_C$ for $x = 0.15$ should be larger than that for $x = 0.30$.

## B. ac magnetization

Figure 6 shows the in-phase ac magnetization $m'$ for $x = 0.15$ (a), 0.25 (b), and 0.30 (c) under acoustic strain. For $x = 0.15$, FM ac magnetization is observed over a wide temperature range owing to non-negligible inhomogeneity, and the midpoint is estimated to be 305 K. Furthermore, the effective hole concentration depends on the oxygen vacancies and Mn vacancies. On the basis of previous reports on $T_C$,[21] the effective hole concentration for the $x = 0.15$ film is assumed to correspond to $x \sim 0.18$, which is on the boundary between the insulating FM and metallic FM phases. For $x = 0.15$ film, which is intrinsically close to the insulating composition,
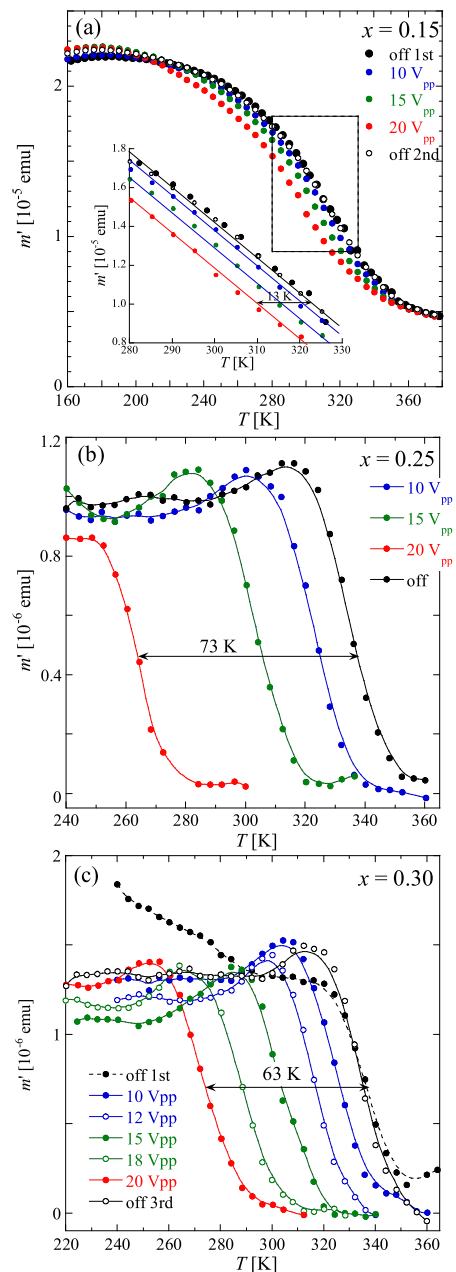


FIG. 6. Temperature dependence of in-phase ac magnetic susceptibility ($m'$) of the $La_{1-x}Sr_xMnO_3$ films with $x = 0.15$ (a), 0.25 (b), and 0.30 (c) as a function of acoustic strain. As for $x = 0.30$, in a series of measurements as $V = 0 \to 5 \to 10 \to 12 \to 0 \to 15 \to 18 \to 20 \to 0$ $V_{pp}$, the data for $V = 5$ $V_{pp}$ state and the second $V = 0$ $V_{pp}$ one (names off the second) are omitted to display systematical change clearly. All three $V = 0$ $V_{pp}$ states exhibit consistency in the temperature region near $T_C$.

$m'$ shifts slightly toward the lower temperature side by yielding acoustic strain, and the magnitude of the reduction, as estimated from the shift of the midpoint, is at most 13 K. For $x = 0.25$ and 0.30, which should be in the metallic phase, an $m'$ value

**FIG. 7**. $V$ dependence of $\Delta T_C$ for the La$_{1-x}$Sr$_x$MnO$_3$ films with $x = 0.15$, 0.25, and 0.30.

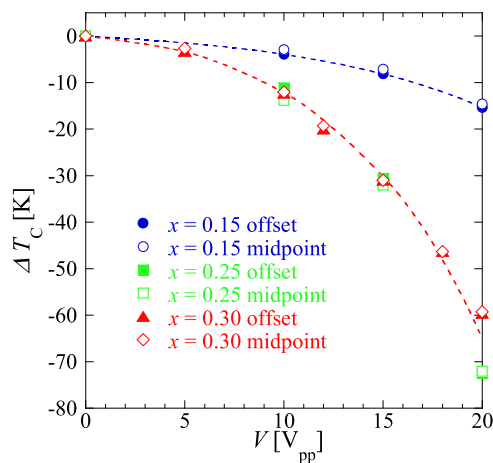corresponding to ferromagnetism appears within a narrow temperature range of approximately 40 K. The midpoints of $m'$ for $x = 0.25$ and 0.30 are 335 K and 338 K, respectively, and the offsets are approximately 350 K. Their $m'$ signals shift toward the lower temperature side with increasing $V$ and maintain their shape despite the change in temperature. For $x = 0.25$ and 0.30, the shift in $m'$ corresponds to $\Delta T_C$ values of 73 K and 63 K at maximum, respectively; these values are more than four times the value of 13 K for $x = 0.15$. These reductions of more than 50 K remarkably overcome the effects of heating due to acoustic strain. It is confirmed that $T_C$ returns to its initial value after $V$ decreases to 0, indicating good reproducibility of the magnetic properties.

Figure 7 shows the $V$ dependence of $\Delta T_C$, which decreases in proportion to $V^2$. There is a distinct difference between the films with near-insulating composition ($x = 0.15$) and metallic composition ($x = 0.25$ and 0.30). The high $T_C$ in the metallic composition region originates from the large charge transfer on the $e_g$ orbital. We believe that energy perturbation by acoustic wave propagation suppresses charge transfer, resulting in the reduction in $T_C$.

## IV. DISCUSSION

The results in Fig. 7 are summarized in Table II, where the effects of acoustic strain are evaluated in terms of the HP and piezo-elastic strain (PES) values. As described in Subsection III B, acoustic strain induces remarkable perturbation effects that result in the suppression of FM ordering. The superior control of $T_C$ in the metallic

films compared to that in the near-insulating film was confirmed by preliminary measurements up to $V = 20$ V$_{pp}$ using powder samples with $x = 0.15$, 0.20, 0.25, and 0.30, for which $\Delta T_C = -9.2$ K, $-27.5$ K, $-17.7$ K, and $-16.8$ K, respectively (see Fig. S1 of the supplementary material). Referring to the previous hydrostatic pressure experiments, the effects of acoustic strain on the films with $x = 0.25$ and 0.30 can be considered to be negative pressure effects corresponding to a pressure of approximately $-20$ GPa. For $x = 0.30$, the acoustic strain effect is considered to correspond to a PES of 2 MV/m. Thus, by applying acoustic strain to the electron conduction system, we could obtain remarkable changes in the thermal stability of the FM ordering.

The unit-cell level of structural change for $x = 0.15$ is qualitatively different from that for $x = 0.30$. The in-plane tension (out-of-plane compression) response of the former involves an increase in unit-cell volume, whereas the hydrostatic compression response of the latter involves a decrease. Indeed, both films show a decrease in $T_C$. Thus, we focus on $\angle$Mn–O–Mn, which indicates the Jahn–Teller distortion of the MnO$_6$ octahedron. According to previous theoretical and experimental studies,[21] as $\angle$Mn–O–Mn approaches 180°, $T_C$ is likely to increase. The acoustic strain in the $x = 0.15$ film causes a decrease in $\angle$Mn–O–Mn, whereas that in the $x = 0.30$ film has almost no effect on $\angle$Mn–O–Mn. According to a previous study of HP compression with d$\angle$Mn–O–Mn/d$P$ = $+0.16°$/GPa in the metallic phase,[22] the magnitude of the decrease in $\angle$Mn–O–Mn at $V = 20$ V$_{pp}$ for $x = 0.15$ corresponds to $-0.3$ GPa.[22] The increase in the Jahn–Teller distortion with decreasing $\angle$Mn–O–Mn suggests that the crystal structure is shifting toward the orthorhombic structure. By contrast, for $x = 0.30$, the Jahn–Teller distortion shows a slight change under acoustic strain. La has a larger ionic radius than Sr. In regions with large amounts of Sr, the structural response to acoustic strain might be small. Here, if the reduction in $\angle$Mn–O–Mn is the main factor that decreases $T_C$, the $\Delta T_C$ value for $x = 0.15$ must be larger than that for $x = 0.30$. However, the $\Delta T_C$ value for $x = 0.30$ is approximately five times that for $x = 0.15$. Thus, we have to consider another explanation.

Acoustic strain results in dynamic perturbation of the crystal structure. However, in the preliminary experiment for the film with $x = 0.25$, $\Delta T_C$ of $-50$ K level in the midpoint and $-60$ K level in the offset was observed under the transverse type of acoustic strain with approximately 17 MHz (Fig. S2 of the supplementary material). Thus, we can easily assume that the scattering of conduction electrons is enhanced under acoustic strain. This situation effectively suppresses charge transfer. According to the experimental literature presenting the relationship between $T_C$ and the resistivity at $T_C$ (see Fig. S3 of the supplementary material), the change in resistivity in the low resistivity region brings about the larger change in $T_C$ than that in the high resistivity region.[11] Thus, the influence of the

**TABLE II**. Strain responses of the La$_{1-x}$Sr$_x$MnO$_3$ films. HP, PES, and AS stand for high-pressure compression, piezo-elastic strain, and acoustic strain, respectively.

| $x$ | Type of experiment | $\Delta T_C$ at 20 V$_{pp}$ (K) | Corresponding HP (GPa) | Corresponding PES (MV/m) | Reference |
|---|---|---|---|---|---|
| $x = 0.15$ | AS | $-13$ | $-1.0$ | . . . | Present work |
| $x = 0.25$ | AS | $-73$ | $-16.2$ | . . . | Present work |
| $x = 0.30$ | AS | $-63$ | $-23.4$ | 2.3 | Present work |

suppression of charge transfer should appear more prominently in higher $T_C$ specimens. The ferromagnetism of La$_{1-x}$Sr$_x$MnO$_3$ is stabilized in the metallic phase by strong Hund coupling between the $e_g$ and $t_{2g}$ orbitals. Both the change in charge transfer and the change in the Jahn–Teller distortion should be considered, as already suggested for La$_{0.8}$Sr$_{0.2}$MnO$_3$.[32] Now, we consider that the remarkable decrease in $\Delta T_C$ of the present metallic La$_{1-x}$Sr$_x$MnO$_3$ films under acoustic strain originates from the suppression of charge transfer in the $e_g$ orbitals.

We are interested in the acoustic strain effect over a wide frequency range, in particular, below 1 MHz. The experiments for low frequencies are future challenges to investigate how the present results are connected with those against the piezo-elastic strain.

## V. CONCLUSION

We controlled the FM ordering of La$_{1-x}$Sr$_x$MnO$_3$ films using acoustic strain. In a metallic film near the insulating phase, increasing the Jahn–Teller distortion decreases $T_C$ by as much as 15 K. In the metallic FM phase with a $T_C$ midpoint of approximately 340 K, the room-temperature FM state was suppressed below 280 K. The reduction in $T_C$ exceeded 60 K despite using polycrystalline films, and it originated from the suppression of charge transfer in the $e_g$ orbitals rather than in a decrease in ∠Mn–O–Mn.

## SUPPLEMENTARY MATERIAL

See the supplementary material for the results of magnetic measurements for the powder samples of La$_{1-x}$Sr$_x$MnO$_3$ with $x$ = 0.15, 0.20, 0.25, and 0.30 under expansion-type of acoustic strain with the frequency of 1 MHz, for the polycrystalline La$_{1-x}$Sr$_x$MnO$_3$ film with $x$ = 0.25 under the transverse type of acoustic strain with approximately 17 MHz, and for the relationship between $T_C$ and resistivity according to the literature.[11]

## REFERENCES

[1] E. Dagotto, T. Hotta, and A. Moreo, Phys. Rep. **344**, 1 (2001).
[2] G. H. Jonker and J. V. Santen, Physica **16**, 337 (1950).
[3] J. F. Mitchell, D. N. Argyriou, C. D. Potter, D. G. Hinks, J. D. Jorgensen, and S. D. Bader, Phys. Rev. B **54**, 6172 (1996).
[4] X. Xiong, B. Dabrowski, O. Chmaissem, Z. Bukowski, S. Kolesnik, R. Dybzinski, C. W. Kimball, and J. D. Jorgensen, Phys. Rev. B **60**, 10186 (1999).
[5] J. Hemberger, A. Krimmel, T. Kurz, K. von Nidda, V. Y. Ivanov, M. Balbashov, and A. Loidl, Phys. Rev. B **66**, 094410 (2002).
[6] P.-G. de Gennes, Phys. Rev. **118**, 141 (1960).
[7] M. Imada, A. Fujimori, and Y. Tokura, Rev. Mod. Phys. **70**, 1039 (1998).
[8] C. Zener, Phys. Rev. **82**, 403 (1951).
[9] J. B. Goodenough, Phys. Rev. **100**, 564 (1955).
[10] Y. Tokura, A. Urushibara, Y. Moritomo, T. Arima, A. Asamitsu, G. Kido, and N. Furukawa, J. Phys. Soc. Jpn. **63**, 3931 (1994).
[11] A. Urushibara, Y. Moritomo, T. Arima, A. Asamitsu, G. Kido, and Y. Tokura, Phys. Rev. B **51**, 14103 (1995).
[12] C. Kwon, M. Robson, K.-C. Kim, J. Gu, S. Lofland, S. Bhagat, Z. Trajanovic, M. Rajeswari, T. Venkatesan, A. Kratz et al., J. Magn. Magn. Mater. **172**, 229 (1997).
[13] I. Gomes, B. Almeida, A. Lopes, J. Araújo, J. Barbosa, and J. Mendes, J. Magn. Magn. Mater. **322**, 1174 (2010).
[14] F. S. Razavi, G. Gross, H.-U. Habermeier, O. Lebedev, S. Amelinckx, G. V. Tendeloo, and A. Vigliante, Appl. Phys. Lett. **76**, 155 (2000).
[15] K. Horiba, A. Maniwa, A. Chikamatsu, K. Yoshimatsu, H. Kumigashira, H. Wadati, A. Fujimori, S. Ueda, H. Yoshikawa, E. Ikenaga et al., Phys. Rev. B **80**, 132406 (2009).
[16] F. Tsui and M. C. Smoak, Appl. Phys. Lett. **76**, 2421 (2000).
[17] H. Y. Hwang, S.-W. Cheong, P. G. Radaelli, M. Marezio, and B. Batlogg, Phys. Rev. Lett. **75**, 914 (1995).
[18] H. Y. Hwang, T. T. M. Palstra, S.-W. Cheong, and B. Batlogg, Phys. Rev. B **52**, 15046 (1995).
[19] J. Fontcuberta, B. Martinez, A. Seffar, S. Piñol, J. L. García-Muñoz, and X. Obradors, Phys. Rev. Lett. **76**, 1122 (1996).
[20] J. Fontcuberta, V. Laukhin, and X. Obradors, Appl. Phys. Lett. **72**, 2607 (1998).
[21] Y. Moritomo, A. Asamitsu, and Y. Tokura, Phys. Rev. B **51**, 16491 (1995).
[22] D. P. Kozlenko, I. N. Goncharenko, B. N. Savenko, and V. I. Voronin, J. Phys.: Condens. Matter **16**, 6755 (2004).
[23] G. Colizzi, A. Filippetti, and V. Fiorentini, Phys. Rev. B **76**, 064428 (2007).
[24] A. J. Millis, T. Darling, and A. Migliori, J. Appl. Phys. **83**, 1588 (1998).
[25] J. Heidler, C. Piamonteze, R. V. Chopdekar, M. A. Uribe-Laverde, A. Alberca, M. Buzzi, A. Uldry, B. Delley, C. Bernhard, and F. Nolting, Phys. Rev. B **91**, 024406 (2015).
[26] Y. Yang, M. M. Yang, Z. L. Luo, H. Huang, H. Wang, J. Bao, C. Hu, G. Pan, Y. Yao, Y. Liu et al., Appl. Phys. Lett. **100**, 043506 (2012).
[27] C. Thiele, K. Dörr, O. Bilani, J. Rödel, and L. Schultz, Phys. Rev. B **75**, 054408 (2007).
[28] R. Nori, S. N. Kale, U. Ganguly, N. R. C. Raju, D. S. Sutar, R. Pinto, and V. R. Rao, J. Appl. Phys. **115**, 033518 (2014).
[29] K. Tsuruta, M. Mito, T. Nagano, Y. Katamune, and T. Yoshitake, Jpn. J. Appl. Phys., Part 1 **53**, 07KC07 (2014).
[30] K. Irie, M. Mito, T. Nagano, K. Tsuruta, and S. Nobukiyo, Jpn. J. Appl. Phys., Part 1 **53**, 07KC05 (2014).
[31] Q. Huang, A. Santoro, J. W. Lynn, R. W. Erwin, J. A. Borchers, J. L. Peng, and R. L. Greene, Phys. Rev. B **55**, 14987 (1997).
[32] T. Kanki, H. Tanaka, and T. Kawai, Phys. Rev. B **64**, 224418 (2001).